A Flow Topology Optimization Method for a Diffuser Using the Lattice Boltzmann Method

Zahra Talebpour
Mechanical Engineering Department, Ferdowsi University of Mashhad, Mashhad, Iran
Talebpour.Zahra@mail.um.ac.ir

Hamid Niazmand
Mechanical Engineering Department, Ferdowsi University of Mashhad, Mashhad, Iran
niazmand@um.ac.ir

Omid Reza Mohammadipour
Mechanical Engineering Department, Payame Noor University, Mashhad, Iran
o.mohammadipour@pnu.ac.ir

Hossein Ajam
Mechanical Engineering Department, Ferdowsi University of Mashhad, Mashhad, Iran
h.ajam@um.ac.ir

Abstract

We consider the optimal design of incompressible fluid flow through a diffuser at low Reynolds numbers. The design problem is solved by a topology optimization approach providing a mechanism to create novel and non-intuitive optimal designs in a mathematical process. While size and shape optimization methods are limited to modifying existing boundaries of an initial design, topology optimization allows to merge and evolve boundaries without requiring an initial guess. Topology optimization of fluid flow is commonly based on a material interpolation approach in geometry representation. Here the solid material is modeled as an artificial porous region to impose zero velocities. Fluid flow is then predicted by the lattice Boltzmann method, which has a simpler numerical formulation than the Navier-Stokes equations and is valid in a larger flow regime. In this paper, the potential of the topology optimization approach is illustrated by a two-dimensional diffuser problem. Moreover, we will show how the domain size may affect the optimum design.

Key words: Flow optimization · Topology optimization · Lattice Boltzmann method · Sensitivity analysis

Nomenclature

f	Distribution function	Greek symbols	
f_i	Discretized distribution function	ε	Design variable (Porosity parameter)
f_i^{eq}	Equilibrium distribution function	δ_u	Convergence criterion for velocity
f_i^{col}	Collided distribution function	δ_ε	Convergence criterion for porosity
N	Number of grid points except the boundaries	ρ	Macroscopic density
p	Pressure	τ	Relaxation time
c_s	Speed of sound	ω_i	Lattice weights
$\vec{u}$	Macroscopic velocity	subscript	
ω	Speed of convergence parameter	i	Lattice node indicator
V	Fluid volume	k	Time step indicator in optimization process

1. Introduction

The optimal control of fluid flows has received considerable attention by engineers and mathematicians, owing to its importance for many technical and scientific applications [1]. Traditionally, design optimization for fluids has focused on shape optimization. The reader is pointed, for example, to the body of work by Jameson [2], and co-workers on shape optimization for external and internal flows and to the work by Mohammadi, Santiago, and co-workers [3, 4] on shape optimization applied to micro-channels and micro-mixers. Shape optimization is generally limited to varying the location of the boundaries, improving the performance of an existing design through the optimization of a parameterized boundary. These limitations can be overcome by applying the concepts of topology optimization to generate complex, often non-intuitive optimal geometries without requiring an initial (close to optimum) design to start with. We refer to the monograph of Bendsøe and Sigmund [5], for an overview of topology optimization methods. Here, the primary difference between shape and topology optimization is illustrated in figure 1.

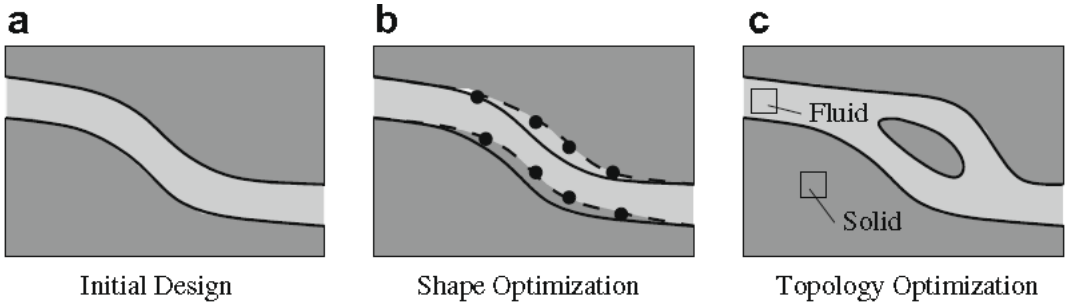

Figure 1: Comparison of shape and topology optimization

In material-based topology optimization, the geometry of a body is represented via an associated material distribution. Thus, each computational node/element is associated with a continuous material description function, which defines if a given node/element contains solid material, fluid, or an intermediate fluid-filled porous material. Although the goal is to find the optimal design without an intermediate material distribution, referred to as ‘‘0-1” design solution, but having a narrow intermediate porous material is also accepted in this method.

Topology optimization of fluids was first introduced by Borrvall and Petersson [6] for Stokes flows employed a porosity method which is similar to the density method in structural optimization of solids. In the porosity method, a design domain is filled with a porous medium and porosity is considered as the design variable. Moreover, the Stokes theory is only valid for flows with a small Reynolds number $Re < 1$. To overcome this limitation, Gersborg-Hansen et al. [7] extended the approach of Borrvall and Petersson [6] to laminar incompressible Navier- Stokes (NS) flows at low Reynolds numbers. Othmer et al. optimized the layout of 3D air duct manifolds employing an incompressible Navier–Stokes model [8, 9]. These approaches are typically based on a finite element or finite volume discretization of the flow equations. Alternatively, Pingen et al. [10-12] presented a topology optimization framework based on steady-state lattice Boltzmann equations (LBE) for computing flow fields. The lattice Boltzmann method is a viable alternative to traditional Navier–Stokes based approaches for fluidic topology optimization. The computational algorithm of LBM is explicit

and simple. Additional advantages of LBM are its simplicity, parallelizability, and applicability beyond hydrodynamics.

In this study, the optimized design of a diffuser at low Reynolds number for different design domain is considered using the method proposed by Yonekura and Kanno [13, 14]. The design domain is represented by a porous medium. The optimization problem is formulated using LBM that solves Boltzmann equations on a lattice grid for approximating low Mach number incompressible viscous flows [15, 16]. As the flow field is solved and the design domain is updated by solving the PDE with respect to flow field variables and porosity, the shape of the design gradually changes. This PDE is formulated using sensitivity analysis for the objective function that updates the design variables, and it depends on a current state of the transient flow field.

The remainder of this paper is organized as follows: In Section 2, the definition of LBM method in porous medium and an optimization problem is introduced. Section 3, reports numerical results and finally, Section 4 concludes this paper.

2.1 Lattice Boltzmann method for flow in porous medium

In this paper, the Bhatnager–Gross–Krook (BGK) model [17, 18] is used for LBM computation, where a fluid is modeled as an assemblage of particles based on kinetic theory. The distribution function of the particles, denoted f_i, is governed by following LBE including local collision and a global propagation step:

$$\text{Collision:} \qquad f_i^{col}(x,t) = f_i(x,t) - \frac{f_i(x,t) - f_i^{eq}(x,t)}{\tau} + \delta t F_i(x,t), \tag{1}$$

$$\text{Propagation:} \qquad f_i(x + e_i, t + \delta t) = f_i^{col}(x,t). \tag{2}$$

Here, $f_i(x,t)$ is defined on each lattice grid at the ith direction, e_i is the direction vector for ith direction depending on the lattice configuration. Furthermore, τ is the relaxation time coefficient, δt is time step size, and $f_i^{eq}(x,t)$ is equilibrium distribution function and $F_i(x,t)$ is an external force term for flow in porous media, which are formulated by Guo and Zhao [19] as

$$f_i^{eq}(x,t) = \omega_i \rho \left[1 + \frac{e_i . u}{c_s^2} + \frac{(u \otimes u) : (e_i \otimes e_i - c_s^2 I)}{2\varepsilon c_s^4}\right] \tag{3}$$

$$F_i(x,t) = \omega_i \rho (1 - \frac{1}{2\tau}) \left[\frac{e_i . \hat{F}}{c_s^2} + \frac{(u \otimes \hat{F}) : (e_i \otimes e_i - c_s^2 I)}{\varepsilon c_s^4}\right] \tag{4}$$

where ω_i represents the weighting factors, the vector u is the velocity vector in the free-stream direction, ρ is the density of the fluid, I is an unit tensor, $\hat{F}$ is an external force vector. We use $\otimes$ to denote the tensor product. In order to avoid divergence in (3) and (4), we restrict $\varepsilon > 1.0e^{-3}$.

In this paper, the two–dimensional, nine velocity vectors at each lattice site, D2Q9, is used. This model is very common, especially for solving fluid flow problems. The speeds are $e_i=0$ for i=0, $e_i = \lambda_i(\cos\theta_i, \sin\theta_i)c$ with $\lambda_i=1$ and $\theta_i=(i-1)\pi/2$ for i=1-4, and $\lambda_i = \sqrt{2}$ and $\theta_i=(i-5)\pi/2+\pi/4$ for i=5-8. Here c is the lattice velocity $c = \delta x/\delta t$ where δx is a lattice spacing. The

weighting factors are given by ω_i=0 for i=0, ω_i=1/9 for i=1-4, ω_i=1/36 for i=5-8. Moreover, c_s is the speed of the sound in lattice units is c /$\sqrt{3}$. The macroscopic parameters in the lattice Boltzmann method such as mass density, redefined velocity in porous media and pressure are evaluated by taking statistical moments of the distribution function f_i, and are given by [20]

$$\rho(x,t) = \sum_{i=0}^{8} f_i, \tag{5}$$

$$\rho(x,t)u(x,t) = \sum_{i=0}^{8} f_i e_i + \frac{\delta t}{2}\rho(x,t)\hat{F}, \tag{6}$$

$$p(x,t) = \rho(x,t)c_s^2, \tag{7}$$

where $p = \rho c_s^2$ is the isothermal ideal gas equation of state for the LBM. It can be shown that the Navier-Stokes equations can be derived from the LBE (1) and (2) through a Chapman-Enskog expansion procedure, in which the kinematic viscosity ν is related to the dimensionless relaxation time as follows:

$$\upsilon = \left(\tau - \frac{1}{2}\right) c_s^2 \delta t. \tag{8}$$

Reynolds number is also computed by

$$\mathrm{Re} = \frac{L\overline{U}}{\upsilon}, \tag{9}$$

where L and $\overline{U}$ are the mean velocity and length in y-direction at the inlet, as characteristic properties, respectively.

2.2 The Optimization Problem

The goal of topology optimization is to modify the shape and connectedness of a domain, such that the desired objective function is minimized. In general terms a topology optimization problem for steady-state flow conditions can be written as follows:

$$\min_{\varepsilon} \mathcal{F}(\vec{u}, \varepsilon), \quad \text{s. t.} \begin{cases} \varepsilon, & \text{subject to design constraints,} \\ \vec{u}, & \text{solves the governing equations for } \varepsilon, \end{cases} \tag{10}$$

where s. t. stands for subject to, ε denotes the design variable, and $\mathcal{F}$ the objective function.

To represent both fluid and non-fluid (solid) regions, we use the porous model due to Borrvall and Petersson [6]. Let ε denotes porosity as a vehicle to smoothly transition between fluid and solid. This porosity model permits a smooth transformation from fluid sites (ε=1) into solid sites (ε=0) and vice versa, leading to a porous layer that represents the fluid-solid interface (with intermediate value of porosity). The external force vector due to the presence of a porous medium utilized in (4) is modeled as the frictional force, i.e., the Brinkman-extended Darcy equation, defined as

$$\hat{F} = -\alpha(\varepsilon)\vec{u}, \tag{11}$$

with the drag coefficient $\alpha(\varepsilon)$ given by

$$\alpha(\varepsilon) = \alpha_0 \underline{\varepsilon} \frac{1-\varepsilon}{\varepsilon + \underline{\varepsilon}}. \tag{12}$$

Here, $\underline{\varepsilon}$ is a positive constant and α_0 is a large constant. Note that α takes a finite value, α_0, at $\varepsilon=0$; if $\varepsilon=1$, then $\alpha=0$ representing the fully fluid region. For example, we use $\alpha_0=1.0\times10^3$ and $\underline{\varepsilon}=1.0\times10^{-5}$ in the numerical experiments.

In this study the objective is to minimize energy dissipation. Energy dissipation functional is sum of viscous dissipation $D(\vec{u}, \varepsilon)$ and frictional dissipation $C(\vec{u}, \varepsilon)$, $\mathcal{F}(\vec{u}, \varepsilon)=D(\vec{u}, \varepsilon)+C(\vec{u}, \varepsilon)$, which are formulated as:

$$D(\vec{u},\varepsilon) = \frac{1}{2}\int_\Omega \varepsilon^p \nu \left\| \nabla\vec{u} + (\nabla\vec{u})^T \right\|^2 dx, \tag{13}$$

$$C(\vec{u},\varepsilon) = -\int_\Omega \hat{F}.\vec{u}\, dx = \int_\Omega \alpha(\varepsilon)\, \|\vec{u}\|^2 dx. \tag{14}$$

Here, Ω denotes a design domain. From a physical point of view, p in (13) should be 0. However, we use $2<p<10$ in order to obtain good convergence of optimization as suggested by Borrvall and Petersson [6]. We use $\|.\|$ to represent the corresponding norm.

The only optimization constraints used in this study are a volume constraint and the range of porosity changes. The volume constraint limits the amount of fluid in the design domain, prescribing that at most a given fraction of the design domain is allowed to be occupied by a fluid, and the remainder must be solid. We define the constraints by

$$0 \le \varepsilon_k(x,t) \le 1, \tag{15}$$

$$\int_\Omega \varepsilon(x,t)dx = V(t), \tag{16}$$

where suffix k is used to show the values at the kth time step, i.e., $t=k\delta t\ \forall\ t\in[0, T]$. $V(t)$ affecting on the convergence profile, is defined by $V(t)=(V_0-V)\exp(-\omega t)+V$, where ω is a constant which controls the speed of convergence.

2.3 Sensitivity Analysis for Topology Optimization

The optimization problem (10) can be solved using gradient-based optimization techniques, where the derivatives of the objectives and constraints are used by the optimization algorithm to determine search directions for a feasible, optimal solution. In this approach the gradient $d\mathcal{F}/d\varepsilon$ drives the objective $\mathcal{F}$ to the local optimal solution $\mathcal{F}_{opt}$. In order to provide the gradients of the objective, we first define the corresponding Lagrangian function as:

$$\mathcal{L}(\vec{u},\varepsilon) = C(\vec{u},\varepsilon) + D(\vec{u},\varepsilon) + \eta_1\varepsilon(x,t) + \eta_2\big(1-\varepsilon(x,t)\big) + \eta_3\Big(\int_\Omega \varepsilon(x,t)dx - V(t)\Big) \tag{17}$$

where η_1, η_2 and η_3 are the Lagrange multipliers. Then, the optimality condition of (10) can be written as follows:

$$\frac{d\mathcal{L}}{d\varepsilon}(x,t) = \frac{d(D+C)}{d\varepsilon}(x,t) + \eta_1 - \eta_2 + \eta_3 \tag{18}$$

At intermediate value of porosity, let $\eta_1=0$, $\eta_2=0$ and $\eta_3= M(t)$. We seek the new value of $\varepsilon(x,t)$ at each time step such that the design domain becomes updated. This can be done by

evaluating $\delta\varepsilon(x,t) = \partial\varepsilon/\partial t\,(x,t) = -\,d\mathcal{L}/d\varepsilon\,(x,t)$ in the form of updating porosity, $\varepsilon_{k+1} = \varepsilon_k + \delta\varepsilon_k$, which is discretized as follows:

$$\varepsilon_{k+1} = \begin{cases} 0 & \text{if } -\kappa\dfrac{d(D+C)}{d\varepsilon}\delta t - M_k \le 0, \\ \varepsilon_k - \kappa\dfrac{d(D+C)}{d\varepsilon}\delta t - M_k & \text{if } 0 < -\kappa\dfrac{d(D+C)}{d\varepsilon}\delta t - M_k < 1, \\ 1 & \text{if } -\kappa\dfrac{d(D+C)}{d\varepsilon}\delta t - M_k \ge 1. \end{cases} \tag{19}$$

The scaling coefficient $\kappa > 0$ relating to the speed of convergence of the porosity method [13, 14], is defined by

$$\max_{\{x|0<\varepsilon(x)<1\}}\left(\kappa\frac{d(D+C)}{d\varepsilon}(x,t)\right) = 0.01. \tag{20}$$

M, a variable in order to control the volume of the fluid at each time step, is computed using the following algorithm.

- Step 1. Compute $\delta\varepsilon^i_{temp} = -\kappa\, d(D+C)/d\varepsilon$ and $\varepsilon^i_{temp} = \varepsilon^i_k + \delta\varepsilon^i_{temp}$ $(i = 1, \dots, N)$ as temporary value based on the previous porosity.
- Assign a number to $\varepsilon_{temp}(x)$ at each grid point so that ε^i_{temp} satisfy $\varepsilon^1_{temp} \le \varepsilon^2_{temp} \le \cdots \le \varepsilon^N_{temp}$ where N is the number of grid points, except the boundaries, satisfying $N\delta t = T$.
- Define $X(\varepsilon^i_{temp}) = (N - i)\delta r$, where δr is a volume corresponding to one cell, denoting the sum of volumes of all cells such that the corresponding component of ε_{temp} is greater than or equals to ε^i_{temp}.
- By using $X(\varepsilon_{temp})$, the integral of ε is expressed as

$$\int \varepsilon_{k+1}dx = \int X(\varepsilon)d\varepsilon = \sum_{M_k<\varepsilon^i_{temp}<1+M_k} (\varepsilon^{i+1}_{temp} - \varepsilon^i_{temp})X(\varepsilon^i_{temp}). \tag{21}$$

- Finally, find M satisfying that (21) is equal to V_{k+1}, then (19) satisfies the volume constraint (16).

At each optimization step, the design variable is $\delta\varepsilon_k$ which affects flow field at the next time step. Hence, the derivative of $\mathcal{F} = D + C$ at the next time step with respect to ε_k (19) can be written by using the chain rule as:

$$\frac{d(D+C)_{k+1}}{d\varepsilon_k} = \frac{\partial(D+C)_{k+1}}{\partial u_{k+1}}\bigg|_\varepsilon \frac{\partial u_{k+1}}{\partial\varepsilon_k} + \frac{\partial(D+C)_{k+1}}{\partial\varepsilon_k}\bigg|_u \tag{22}$$

To solve the sensitivity equation (21), requires the evaluation of three partial derivatives: $\partial(D+C)_{k+1}/\partial u_{k+1}$, $\partial u_{k+1}/\partial\varepsilon_k$ and $\partial(D+C)_{k+1}/\partial\varepsilon_k$ which are evaluated based on analytically derived expressions. For the first and third components, we have:

$$\frac{\partial(D+C)_{k+1}}{\partial u_{k+1}}\bigg|_\varepsilon = \varepsilon_k^p \nu\Delta u_{k+1}(u_k,\varepsilon_k)\delta r + 2\alpha u_{k+1}(u_k,\varepsilon_k)\delta r, \tag{23}$$

$$\left.\frac{\partial(\mathrm{D}+\mathrm{C})_{k+1}}{\partial\varepsilon_k}\right|_{\mathrm{u}} = \frac{p}{2}\varepsilon_k^{p-1}\,\nu\left\|\nabla \mathrm{u}_k + (\nabla \mathrm{u}_k)^{\mathrm{T}}\right\|^2 \delta\mathrm{r} + \frac{\mathrm{d}\alpha}{\mathrm{d}\varepsilon_k}\|\mathrm{u}_k\|^2\delta\mathrm{r}. \tag{24}$$

Here, $\mathrm{u}_{k+1}(\mathrm{u}_k, \varepsilon_k)$ in (23) can be computed by LB equations after updating the design variable. Since we assume that the flow field becomes steady at the final step t=T and Reynolds number is small, $\mathrm{u}_{k+1}(\mathrm{u}_k, \varepsilon_k)$ can be approximated by u_k depending on u_{k-1} and ε_k. Then, we have (23) as

$$\left.\frac{\partial(\mathrm{D}+\mathrm{C})_{k+1}}{\partial\mathrm{u}_{k+1}}\right|_{\varepsilon} \simeq \varepsilon_k^p \nu\Delta\mathrm{u}_k(\mathrm{u}_{k-1}, \varepsilon_k)\delta\mathrm{r} + 2\alpha\mathrm{u}_k(\mathrm{u}_{k-1}, \varepsilon_k)\delta\mathrm{r}. \tag{25}$$

To evaluate the second partial derivative in (22), it should be noted that the velocity u_{k+1} is a function of both porosity and distribution functions. However, by using the chain rule, we have

$$\frac{\partial \mathrm{u}_{k+1}}{\partial\varepsilon_k} = \sum_{\mathrm{i}=0}^{8} \frac{\partial \mathrm{u}_{k+1}}{\partial \mathrm{f}_\mathrm{i}(\mathrm{x}, \mathrm{t}+\delta\mathrm{t})}\frac{\partial \mathrm{f}_\mathrm{i}(\mathrm{x}, \mathrm{t}+\delta\mathrm{t})}{\partial\varepsilon_k}, \tag{26}$$

The first component of the right-hand side is obtained from the definitions (5), (6) and (11) as:

$$\frac{\partial u}{\partial \mathrm{f}_\mathrm{i}} = \frac{\left(\frac{\mathrm{e}_\mathrm{i}}{1+\alpha\,\delta t/2} - u\right)}{\rho}. \tag{27}$$

From the LB equations (1) and (2), f_i is differentiated with respect to ε as follows:

$$\frac{\partial \mathrm{f}_\mathrm{i}(\mathrm{x}, \mathrm{t}+\delta\mathrm{t})}{\partial\varepsilon_k} = \frac{\partial \mathrm{f}_\mathrm{i}^{\mathrm{col}}(\mathrm{x}-\delta\mathrm{te}_\mathrm{i}, \mathrm{t})}{\partial\varepsilon_k} = \frac{1}{\tau}\frac{\partial \mathrm{f}_\mathrm{i}^{\mathrm{eq}}(\mathrm{x}-\delta\mathrm{te}_\mathrm{i}, \mathrm{t})}{\partial\varepsilon_k} + \delta\mathrm{t}\frac{\partial \mathrm{F}_\mathrm{i}(\mathrm{x}-\delta\mathrm{te}_\mathrm{i}, \mathrm{t})}{\partial\varepsilon_k}, \tag{28}$$

$$\frac{\partial \mathrm{f}_\mathrm{i}^{\mathrm{eq}}(\mathrm{x}, \mathrm{t})}{\partial\varepsilon_k} = -\omega_\mathrm{i}\rho\frac{(\mathrm{u}_k \otimes \mathrm{u}_k) : (\mathrm{e}_\mathrm{i} \otimes \mathrm{e}_\mathrm{i} - \mathrm{c}_\mathrm{s}^2\mathrm{I})}{2\mathrm{c}_\mathrm{s}^4}\frac{1}{\varepsilon_k^2}, \tag{29}$$

$$\frac{\partial \mathrm{F}_\mathrm{i}(\mathrm{x}, \mathrm{t})}{\partial\varepsilon_k} = -\omega_\mathrm{i}\rho\left(1-\frac{1}{2\tau}\right)\left[\frac{\mathrm{e}_\mathrm{i}.\mathrm{u}_k}{\mathrm{c}_\mathrm{s}^2}\frac{\partial\alpha_\mathrm{k}}{\partial\varepsilon_k} + \frac{(\mathrm{u}_k \otimes \mathrm{u}_k) : (\mathrm{e}_\mathrm{i} \otimes \mathrm{e}_\mathrm{i} - \mathrm{c}_\mathrm{s}^2\mathrm{I})}{\mathrm{c}_\mathrm{s}^4}\frac{\partial}{\partial\varepsilon_k}\left(\frac{\alpha_\mathrm{k}}{\varepsilon_k}\right)\right]. \tag{30}$$

The convergence of the LBM time-marching scheme toward steady-state flow solutions is achieved when $|\vec{\mathrm{u}}_{k+1} - \vec{\mathrm{u}}_k| < \delta_\mathrm{u}$. The optimization algorithm also terminates, if the maximum change in the design variable is less than δ_ε, i.e., $|\varepsilon_{k+1} - \varepsilon_k| < \delta_\varepsilon$. While this stopping criteria for monitoring the convergence does not guarantee that the optimality conditions are satisfied, numerical studies have shown that it is practical and sufficient to obtain visually smooth boundaries of the desired accuracy, and the geometry does not change noticeable even if more iterations are performed. In the current study, the thresholds are defined $\delta_\mathrm{u} = 1.0\mathrm{e}^{-3}$ and $\delta_\varepsilon = 1.0\mathrm{e}^{-4}\delta\mathrm{r}$.

3. Numerical implementation (a Diffuser (2D))

The diffuser optimization problem, similar to that found in [6], is considered over the system while the volume fraction of fluid is restricted to at most 50%, which is equivalent to value used by Borrvall and Petersson [6]. The Reynolds number is set to Re=10.0 and the

design domain is discretized by 101 grid points in both x and y directions. The problem setup and the boundary conditions are shown in figure 2. The parabolic velocity distribution at the inlet and outlet is specified as

$$u_{in}(y) = -6\bar{U}\frac{y(y-L)}{L^2}$$
$$u_{out}(y) = -6\times 27\bar{U}\frac{\left(y-\frac{L}{3}\right)\left(y-\frac{2L}{3}\right)}{L^2} \qquad \text{for } y \in \left\{y \middle| \frac{L}{3} \le y \le \frac{2L}{3}\right\}. \tag{31}$$

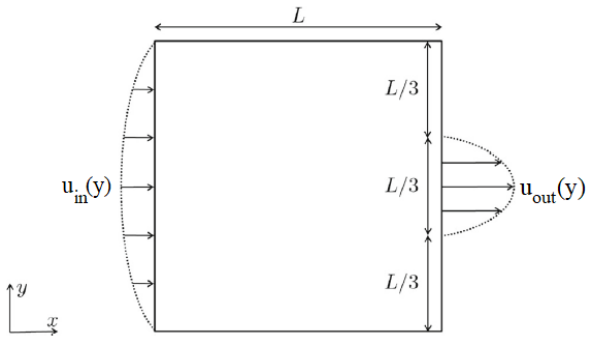

Figure 2: Diffuser design domain with inlet and outlet conditions

To verify the accuracy of the performance of topology optimization algorithm, the obtained result are compared against the one of Borrvall and Petersson [6]. According to fig. 3, one can see that the results are similar. Figure 4 shows a good convergence pattern of the objective value, i.e., the summation of viscous dissipation D and frictional dissipation C, as the number of iterations. It should be noted that, the red region corresponds to fully fluid region, and blue region to fully solid region.

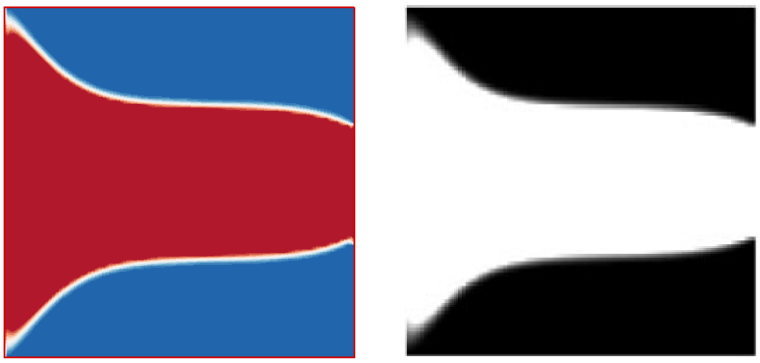

Figure 3: Optimal design for a diffuser at Re=10 on a 100 × 100 lattice (left) in this paper (right) in [6]

In this study, it is also investigated that how different domain aspect ratios with a constant value of lattice nodes (e.g. 10,000), and constant value of the specified volume of the flow domain can affect the objective values. The initial and final objective values (energy dissipation), and the final values of viscous and frictional dissipation of the optimized designs of a diffuser at Re=10.0 with $\bar{V} = 0.5|\Omega|$ are presented in table 1. From the results it can be seen that increasing the height and decreasing the length of the domain leads to low value of the objective function due to the decreased effect of viscosity rather than the case of 200 × 50.

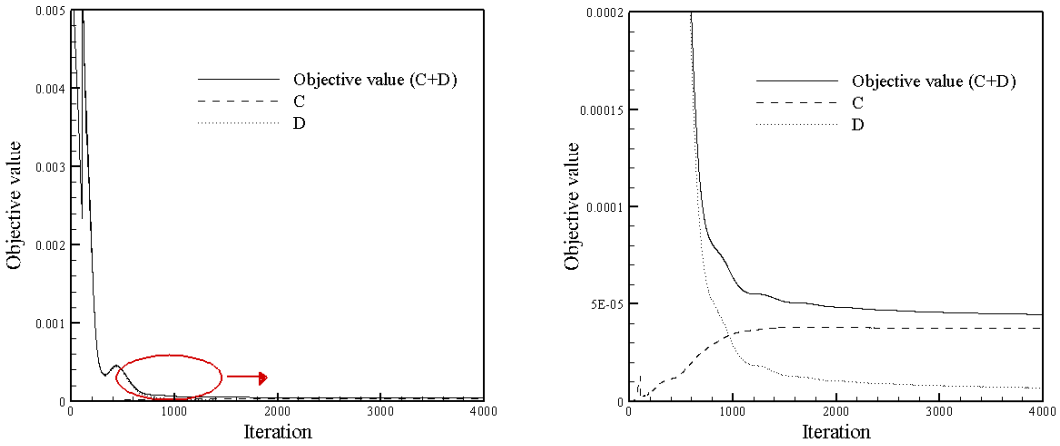

Figure 4: Convergence pattern of the objective function for the diffuser

Table 1: Comparison of optimization results for different lattice sizes with constant number of lattice nodes at Re = 10

Lattice size	Initial Objective	Final Objective	Viscous Dissipation	Frictional Dissipation
50 × 200	$2.429160e^{-3}$	$1.556770e^{-5}$	$1.264534e^{-5}$	$0.2922355e^{-5}$
100 × 100	$5.933506e^{-3}$	$4.512863e^{-5}$	$3.957757e^{-5}$	$0.5551064e^{-5}$
200 × 50	$19.197289e^{-3}$	$40.298171e^{-5}$	$34.034342e^{-5}$	$6.2638283e^{-5}$

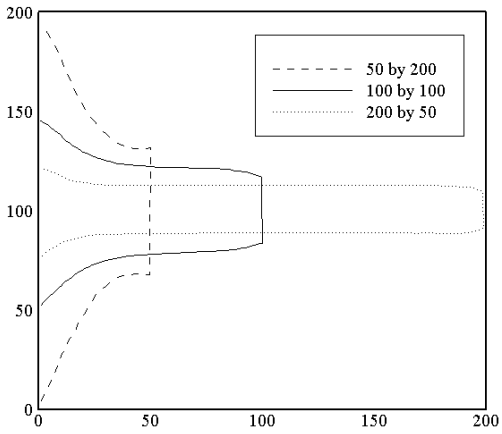

Figure 5: Optimum Diffuser with different domain aspect ratios and constant $\overline{V}$

Figure 5 illustrates the final results for the optimum diffuser design corresponding to three mentioned aspect ratios. In addition to the different final objective values were reported for these cases, the final design topologies around the outlet boundary for the 50 × 200 lattice is different.

4. Conclusions

- An optimization approach to fluid flow based on the lattice Boltzmann method has presented.

- A numerical study has illustrated how the topology optimization can be employed to make an optimized shape for a diffuser without an initial design.
- Finally, the results have obtained and discussed for a 2-dimensional diffuser problem in a three kinds of a design domain leading to shapes with different values of energy dissipation.

References

[1] Gunzburger M. D., 2003, Perspectives in flow control and optimization. Advances in Design and Control, Society for Industrial and Applied Mathematics (SIAM), Philadelphia, PA

[2] Jameson A., 1988, Aerodynamic design via control theory, Journal of Scientific Computing, vol. 3, pp. 233–260.

[3] Ivorra B., Hertzog D. E., Mohammadi B. and Santiago J. G., 2005, Semi-deterministic and genetic algorithms for global optimization of microfluidic protein-folding devices, International Journal for Numerical Methods in Engineering, vol. 66, pp. 319–333.

[4] Molho J. I., Herr A. E., Mosier B. P., Santiago J. G., Kenny T. W., Brennen R. A., Gordon G. B. and Mohammadi B., 2001, Optimization of turn geometries for microchip electrophoresis, Analytical Chemistry, vol. 73, pp. 1350– 1360.

[5] Bendsøe, M.P. and Sigmund O., 2003, Topology Optimization: Theory, Methods, and Applications, Springer-Verlag, Berlin.

[6] Borrvall T. and Petersson J., 2003, Topology optimization of fluids in Stokes flow, International Journal Numerical Methods Fluids, vol. 41, pp. 77–107.

[7] Gersborg-Hansen A., Sigmund O. and Haber R., 2005, Topology optimization of channel flow problems, Structural and Multidisciplinary Optimization, vol. 30, pp. 181–192.

[8] Othmer C., 2006, CFD topology and shape optimization with adjoint methods, VDI Fahrzeug- und Verkehrstechnik, 13. International congress, Berechnung und Simulation im Fahrzeugbau, Würzburg.

[9] Othmer C., de Villiers E. and Weller H. G., 2007, Implementation of a continuous adjoint for topology optimization of ducted flows, 18th AIAA computational fluid dynamics conference. Miami, FL: AIAA.

[10] Pingen G., Evgrafov A. and Maute K., 2007, Topology optimization of flow domains using the lattice Boltzmann method, Structural and Multidisciplinary Optimization, vol. 34, pp. 507–524.

[11] Pingen G., Evgrafov A. and Maute K., 2009, Adjoint parameter sensitivity analysis for the hydrodynamic lattice Boltzmann method with applications to design optimization, Computational Fluids, vol. 38, pp. 910–923.

[12] Pingen G. and Maute K., 2010, Optimal design for non-Newtonian flows using a topology optimization approach, Computer and Mathematics with Applications, vol. 59, pp. 2340–2350.

[13] Yonekura K. and Kanno Y., 2015, A flow topology optimization method for steady state flow using transient information of flow field solved by lattice Boltzmann method, Structural and Multidisciplinary Optimization, vol. 51, pp. 159–172.

[14] Yonekura K. and Kanno Y., 2016, Erratum to: A flow topology optimization method for steady state flow using transient information of flow field solved by lattice Boltzmann method, Structural and Multidisciplinary Optimization, vol. 54, pp. 193–195.

[15] Succi S., 2001, The lattice Boltzmann equation: for fluid dynamics and beyond. Oxford University Press.

[16] Mattila K., Hyväluoma J., Timonen J. and Rossi T., 2008, Comparison of implementations of the lattice-Boltzmann method, Computer and Mathematics with Applications, vol. 55, pp. 1514–1524.

[17] Bhatnagar P. L., Gross E. P. and Krook M., 1954, A Model for Collision Processes in Gases. I. Small Amplitude Processes in Charged and Neutral One-Component Systems, Physical Review, vol. 94, pp. 511– 525.

[18] Pingen G., Evgrafov A. and Maute K., 2007, Topology Optimization of Flow Domains Using the Lattice Boltzmann Method, Structural and Multidisciplinary Optimization, vol. 36, pp. 507–524.

[19] Guo Z. and Zhao T.S., 2002, Lattice Boltzmann model for incompressible flows through porous media, Physical Review, vol. 66, pp. 036–304.

[20] Guo Z., Zheng C. and Shi B., 2002, Discrete lattice effects on the forcing term in the lattice Boltzmann method, Physical Review, vol. 65, pp. 046308-6.